Effectiveness of numerical techniques for calculating the quantity of calcium ion species during calcium sparksin heart muscle

D. A. Lott
Departments of Mathematics and Biotechnology,
Delaware State University, Dover, DE 19901 and
Center for Applied Mathematics and Statistics,
New Jersey Institute of Technology, Newark, NJ 07102,
(302) 857-7059, dlott@desu.edu

M. Li
Department of Mathematical Sciences,
New Jersey Institute of Technology, Newark, NJ 07102

J. R. Berlin
Department of Pharmacology and Physiology, University of
Medicine and Dentistry of New Jersey, Newark, NJ 07102,
(973) 972-1618, berlinjr@umdnj.edu

CAMS Report 0405-01, Fall 2004
Center for Applied Mathematics and Statistics

Effectiveness of numerical techniques for calculating the quantity of Ca^{2+} species during calcium sparks in heart muscle

D. A. Lott[1], M. Li[2] and J. R. Berlin[3]

Abstract

An efficient numerical algorithm based on the convolution of functions and on finite difference approximations for the diffusion equation is utilized to determine the quantity of calcium ions (Ca^{2+}) participating in unitary Ca^{2+} release events, termed "Ca^{2+} sparks," in heart muscle. Output images of localized increases in cytosolic Ca^{2+} concentration ($[Ca^{2+}]$), due predominantly to Ca^{2+} release from intracellular storage sites, are obtained using fluorescent calcium indicators and confocal microscopy. To obtain the quantity of Ca^{2+} underlying these localized increases of cytosolic $[Ca^{2+}]$, one-dimensional output images are deconvolved with a point spread function that describes the optical properties of the microscope. The resulting input image is then reconstructed, assuming symmetry, in a three-dimensional image of $[Ca^{2+}]$ and all Ca^{2+}-bound species. Temporal information about free and bound Ca^{2+} species can be obtained by performing convolutions on a series of output images recorded in time and then accounting for the kinetics of Ca^{2+} interactions with the fluorescent calcium indicator and other Ca^{2+} binding species. The effect of microscope imaging properties on measurements of local $[Ca^{2+}]$ and the ability to reconstruct the underlying changes in Ca^{2+} species during a Ca^{2+} spark are presented.

Keywords: calcium, diffusion, microscopy, reaction-diffusion equations, image reconstruction

1 Introduction

In this paper, we present effective numerical methods to calculate the amount of Ca^{2+} release from the sarcoplasmic reticulum, and its subsequent diffusion in cardiac myocytes using a reaction-diffusion equation governing calcium movements. Our problem, posed as a parabolic system of partial differential equations is treated by an explicit second-order finite difference scheme which is first order in time and second order in space. The mathematical problem determines the $[Ca^{2+}]$ inside the cell from experimental data as well as the change in total Ca^{2+} due to buffering and diffusion. The calculated change in Ca^{2+} is then a critical factor in understanding how excitation-contraction coupling functions in normal and pathological states of the heart.

Excitation-contraction coupling in mammalian heart muscle cells depends on a transient increase in cytosolic $[Ca^{2+}]$ that involves a large release of Ca^{2+} from cytosolic storage sites,

[1]Departments of Mathematics and Biotechnology, Delaware State University, Dover, DE 19901 and Center for Applied Mathematics and Statistics, New Jersey Institute of Technology, Newark, NJ 07102, (302) 857-7059 (p), *dlott@desu.edu*

[2]Department of Mathematical Sciences, New Jersey Institute of Technology, Newark, NJ 07102

[3]Department of Pharmacology and Physiology, University of Medicine and Dentistry of New Jersey, Newark, NJ 07102, (973) 972-1618 (p), *berlinjr@umdnj.edu*

the sarcoplasmic reticulum (SR) and small influx of Ca^{2+} in response to cell membrane depolarization (Figure (1)). This coupling process is believed to occur at specialized subcellular junctions in which Ca^{2+} permeable ion channels located in the cell membrane (SL) termed "L-type Ca^{2+} channels" (or dihydropyridine receptors (DHPR)), come into close apposition with a second group of Ca^{2+} channels located in the sarcoplasmic reticulum membrane, termed "ryanodine receptors" (RYR) or "Ca^{2+} release channels" (Figure (2)).

The space, 20–100 nanometers (nm), and the time, 10–30 milliseconds (msec), in which coupling and Ca^{2+} release occurs is too small to obtain a direct measure of the quantities and fluxes of Ca^{2+} during this process. Further complicating the quantification of Ca^{2+} is the preponderance of Ca^{2+} buffering species in the cytosolic environment. Endogenous Ca^{2+} buffering occurs predominantly to immobile proteins [2]. In addition, diffusible Ca^{2+} chelating molecules, introduced experimentally, can substantially add to the buffering capacity of the cytosol. One of these exogenous Ca^{2+} buffers, B_e, creates upon Ca^{2+} binding a fluorescent species, CaB_e, that is experimentally measured during the coupling process. Thus, although localized excitation-contraction coupling can be observed using light microscopy techniques, experimental observations yield a very inaccurate measure of the total Ca^{2+} participating is this process.

Given the limitations of experimental observations, termed "Ca^{2+} sparks," as a measure of excitation-contraction coupling, reaction diffusion equations have been used to describe the movements of Ca^{2+}; for example, free Ca^{2+}, and Ca^{2+} bound to the various buffering species in the presence of an isotropic myoplasm containing endogenous stationary, endogenous mobile and experimentally introduced mobile (exogenous) buffers [3, 9, 12]. The concentration of free Ca^{2+} is determined by the association and dissociation rates in the presence of buffering species. The effect is to distribute Ca^{2+} between mobile and immobile pools; that is, mobile buffers carry Ca^{2+} along while immobile buffers immobilize Ca^{2+}. The use of exogenous buffers can reduce the effect of endogenous buffers and speed up the transport of Ca^{2+}. Thus, the spread of Ca^{2+} away from the release and influx sites is governed by the reaction-diffusion equations in the presence of Ca^{2+} buffers.

Several important issues relating to the effectiveness with which experimental data can be applied to these mathematical and numerical techniques have received considerably less attention. As part of the validation of our numerical solutions, we study (1) the effectiveness and accuracy of the numerical technique (2) the accuracy of deconvolution on idealized and experimental data, (3) the accuracy of deconvolution with realistic noise contributions included, and (4) the effects of idealizing data versus filtering of experimental data for the determination of quantities of Ca^{2+} involved in Ca^{2+} sparks.

It is well known that deconvolving data is an ill-posed problem and its solution through matrix inversion is not a numerically stable technique. However, the solution of the deconvolved data is in fact the true quantity of the calcium-bound buffer compound and for the physiologist, it is essential to acquire this value. Deconvolution via matrix inversion is the only viable technique given the limitations of experimental measurements. Hence, with the instability of this numerical technique in mind, we use careful analysis to show that matrix inversion for deconvolution leads to an acceptable error. We carry out a careful validation of our methods, described below.

This work may be regarded as a first step toward verifying the utility of these numerical techniques for treating three dimensional, axisymmetric Ca^{2+} sparks. This method must be used with great care, however, to prevent solutions from degrading due to propagating numerical errors.

We present examples showing that our numerical method is effective, efficient and accurate. Due to the nonlinearity of the equations, a closed-form, analytic solution is not available with which to compare the computed solution. Moreover, there are no available error estimates for the nonlinear system. Consequently, we must carry out a rather intricate program, in which numerical linear algebra plays a central role, to validate our results:

Step (i). Compute the average Ca^{2+} spark from experimental data.

Step (ii). Deconvolve observed image to determine the deblurred fluorescent intensities.

Step (iii). Interpolate this data to include data at smaller intervals.

Step (iv). Convert the fluorescent intensities into concentrations of calcium-bound exogenous buffers.

Step (v). Compute the total amount of Ca^{2+} using the reaction-diffusion model which governs the event.

The development of this algorithm gives rise to numerical schemes capable of handling non-smooth data, which is a by-product of the experimental results obtained. Section 2 gives a brief formulation of the reaction-diffusion problem of calcium release. In subsequent sections, we carry out steps (i)–(v) and address issues regarding utilities of this technique.

2 Problem Formulation

In order to calculate the amounts of Ca^{2+} participating in a Ca^{2+} spark, we must account for Ca^{2+} and all species of Ca^{2+} buffers in the cytosolic space, their diffusion and the kinetics of their Ca^{2+} binding reactions. The computational domain consists of a sphere of radius $\rho = 3.3\mu$m for $t \leq 46$ msec, the time of experimental observation. We also assume isotropic diffusion on all dimensions even though the geometry of the cytosolic environment accessible to Ca^{2+} and these buffers is complex. This assumption allows us to simplify the transport equations to a one dimensional problem. We define Ca^{2+} buffering species as endogenous stationary (B_s), mobile (B_m) and exogenous, mobile (B_e) in keeping with the nomenclature of previous studies [12]. The reaction-diffusion equations are defined as:

$$\begin{aligned}\frac{\partial [Ca^{2+}]}{\partial t} &= D_{Ca} \bigtriangledown^2 [Ca^{2+}] - k_s^+ [Ca^{2+}][B_s] + k_s^- [CaB_s] \\ &\quad -k_m^+ [Ca^{2+}][B_m] + k_m^- [CaB_m] \\ &\quad -k_e^+ [Ca^{2+}][B_e] + k_e^- [CaB_e], \end{aligned} \tag{1}$$

$$\frac{\partial [B_m]}{\partial t} = D_{B_m} \bigtriangledown^2 [B_m] - k_m^+ [Ca^{2+}][B_m] + k_m^- [CaB_m], \quad (2)$$

$$\frac{\partial [B_e]}{\partial t} = D_{B_e} \bigtriangledown^2 [B_e] - k_e^+ [Ca^{2+}][B_e] + k_e^- [CaB_e], \quad (3)$$

$$\frac{\partial [CaB_s]}{\partial t} = k_s^+ [Ca^{2+}][B_s] - k_s^- [CaB_s], \quad (4)$$

$$\frac{\partial [CaB_m]}{\partial t} = D_{CaB_m} \bigtriangledown^2 [CaB_m] + k_m^+ [Ca^{2+}][B_m] - k_m^- [CaB_m], \quad (5)$$

$$\frac{\partial [CaB_e]}{\partial t} = D_{CaB_e} \bigtriangledown^2 [CaB_e] + k_e^+ [Ca^{2+}][B_e] - k_e^- [CaB_e], \quad (6)$$

subject to buffer reactions:

$$B_i + Ca^{2+} \underset{k_i^-}{\overset{k_i^+}{\rightleftharpoons}} CaB_i \quad (7)$$

and the conservation condition

$$[B_i]_T = [B_i] + [CaB_i] \quad (8)$$

since the initial total concentration of mobile buffer is spatially uniform when $D_{B_i} = D_{CaB_i}$. Hence the total calcium is computed using

$$[Ca^{2+}]_T = [Ca^{2+}] + [CaB_s] + [CaB_m] + [CaB_e], \quad (9)$$

In the above equations, $k_i^{\pm}$ are the association and dissociation rate constants, and D_{Ca}, D_{B_m}, D_{B_e}, D_{CaB_m} and D_{CaB_e} are the diffusion constants for free Ca^{2+}, the mobile endogenous buffer, the mobile exogenous buffer, and Ca^{2+} bound to mobile endogenous buffer, respectively. Note that these equations contain five time scales; that is, 2 time scales of the buffering and 3 times scales of diffusion.

Ideally, one would measure the concentrations of Ca^{2+} and Ca^{2+}-bound buffering species to quantitate the total amount to Ca^{2+} involved in the evolution of a Ca^{2+} spark. However, experimentally, only the amount of CaB_e can be observed. As a result, we are forced to utilize $[CaB_e]$ in space and time as input to estimate the concentration of free Ca^{2+} in equation (1) and the quantities of all other buffering species (CaB_s and CaB_m) involved in this system (equations (2) – (5)) to solve for the total amount of Ca^{2+}. Thus, the solutions to these reaction-diffusion equations are the object of our numerical study.

3 Method

The quantity of calcium species in heart muscle is determined using a five-step algorithm, defined below.

Step (i): Computation of average Ca^{2+} spark data

Of interest, is the determination of effects of cytosolic calcium buffering on local calcium signaling in cardiac muscle. Intracellular Ca^{2+} is measured after injection of a Ca^{2+}-sensitive fluorescent dye (fluo-3) into single cardiac ventricular myocytes. Injected myocytes are then imaged with high numerical aperture optics on a laser scanning confocal microscope. Fluorescence intensity is measured using a so-called "line scan" technique where data are acquired along a single raster line (that is, in one dimension) at 2 msec intervals to build up images in space (x) and time (t). Experimental signal-to-noise ratios of these images are typically on the order of 2-to-1 so that the average images are constructed (in this report, Ca^{2+} sparks are the average of more than 60 separate images) where each image is aligned in space and time by the maximal fluorescence intensity. Note that the physical domain is three dimensional and axisymmetric. This symmetry allows a three dimensional, spherical mass of calcium to be reduced numerically to one dimension for calculation. Three dimensionality is recovered after mass diffusion and total calcium concentration is obtained.

The experimental conditions were set by including 0.82 millimolar (mM) fluo-3, defined as B_e, and 4.7 mM EGTA, defined as B_m, in the cell with resting [Ca^{2+}] set to 100 nanomolar (nM) [4]. The resolution limit of the microscope is approximately 0.4 micrometers (μm) in the x-axis. Since Ca^{2+} spark occurs on the scale of 0.1 μm, this event cannot be observed clearly under the microscope. The microscope image is a distortion of the actual object. Consequently, we have to utilize numerical techniques to generate mathematical models that will represent this event.

Step (ii): Blurring and Deblurring via deconvolution

The limited resolution of the optical microscope results in an inaccurate or "blurred" image of the Ca^{2+} spark. Nonetheless, blurring can be estimated by measuring the ability of the system to image known objects whose dimensions are smaller than the resolution of the microscope. In this case, 0.1 μm fluorescent beads were used to construct a point spread function (PSF) describing the imaging properties of the microscope.

Blurring is simulated as follows [5]: Let $F(X, Y, Z)$ be the observed fluorescence of CaB_e, the mobile exogenous calcium-bound buffer as seen via the microscope. Let $f(x, y, z)$ be the true object fluorescence which is assumed to be spherically symmetric with respect to the center of the spark and $P(X, Y, Z)$ be the point spread function (PSF) describing the blurring effects of a specific microscope. Then

$$F(X,Y,Z) = \int_{-\infty}^{\infty}\int_{-\infty}^{\infty}\int_{-\infty}^{\infty} f(x,y,z)P(x-X, y-Y, z-Z)\,dx\,dy\,dz \tag{10}$$

defines the fluorescent intensity of the spark at any point (X, Y, Z). For simplicity, assume that we process Ca^{2+} sparks on the center of scanning line of the microscope where $Y = Z = 0$. Hence,

$$F(X) = \int_{-\infty}^{\infty}\int_{-\infty}^{\infty}\int_{-\infty}^{\infty} f(x,y,z)P(x-X, y, z)\,dx\,dy\,dz. \tag{11}$$

We then assume that the PSF is a separable product of three Gaussian functions $G(x)$, $G(y)$ and $H(z)$,

$$\begin{aligned} G(x) &= \exp(-x^2/\sqrt{2}\sigma_{xy}) && (12)\\ G(y) &= \exp(-y^2/\sqrt{2}\sigma_{xy}) && (13)\\ H(z) &= \exp(-z^2/\sqrt{2}\sigma_{z}) && (14) \end{aligned}$$

where σ_{xy} and σ_x are the standard deviations for the functions $G(x)$ and $H(z)$, respectively. We appropriately define the true fluorescent spark to be

$$\begin{aligned} f(x,y,z) &= f_\rho(0)\exp(-\rho^2/2\sigma^2) && (15)\\ &= f_\rho(0)g(x)g(y)g(z) && (16) \end{aligned}$$

for $\rho^2 = x^2 + y^2 + z^2$, where the maximum fluorescent intensity is defined by $f_\rho(0)$. At any point (X, Y) in any focal plane Z, the observed image is the sum of contributions from the entire specimen volume weighted by the PSF. Combining equations (11) – (16), we obtain the observed fluorescent intensity of the spark in one dimension as

$$F(X) = f_\rho(0)\int_{-\infty}^{\infty} g(x)G(x-X)\,dx \int_{-\infty}^{\infty} g(y)G(y)\,dy \int_{-\infty}^{\infty} g(z)H(z)\,dz. \qquad (17)$$

Now, define the following:

$$\begin{aligned} J &= \int_{-\infty}^{\infty} g(y)G(y)\,dy && (18)\\ L &= \int_{-\infty}^{\infty} g(z)H(z)\,dz. && (19) \end{aligned}$$

Thus we can rewrite equation (17) as

$$F(X) = f_\rho(0)J\ L\int_{-\infty}^{\infty} g(x)G(x-X)\,dx \qquad (20)$$

where

$$\begin{aligned} F(X) &= \int_{-\infty}^{\infty} \tilde{g}(x)G(x-X)\,dx && (21)\\ \tilde{g}(x) &= f_\rho(0)J\ Lg(x) && (22) \end{aligned}$$

is a basic convolution defined by

$$F(X) = \tilde{g}(X) * G(X). \qquad (23)$$

This convolution is computed using a finite approximation to the integral. Given a partition of the interval $(-\infty, \infty)$ such that for $x_k = k * \triangle x$

$$\ldots < -x_N < -x_{N-1} < \ldots < -x_1 < x_0 < x_1 < \ldots < x_{N-1} < x_N < \ldots, \qquad (24)$$

$$F(X) = \int_{-\infty}^{\infty} \tilde{g}(x)G(x-X)\,dx \tag{25}$$

$$F(X) = \lim_{N\to\infty} \sum_{k=-N}^{N} \tilde{g}(x_k)G(x_k - X). \tag{26}$$

Equation (26) can be expressed in matrix form as

$$F(\mathbf{x}) = G(\mathbf{X}-\mathbf{x})\tilde{g}(\mathbf{x}) \tag{27}$$

where X, x denote the vectors of values of X and x, $x_k = x(k)$ and $\mathbf{G}$ is symmetric such that $\mathbf{G}(x_0)$ is the diagonal entry.

We solve equation (27) by usual numerical techniques for matrix inversion; that is, Crout factorization to determine values of $\tilde{g}(\mathbf{x})$, which represents the the calcium-bound mobile exogenous buffer in space.

Step (iii): Cubic Spline Interpolation

Since the microscope takes discrete images at every $\triangle t$ time step, we must insure that the time step utilized by the reaction-diffusion equation is restricted by the Courant-Friedrichs-Lewy condition (CFL number) [8]. The CFL condition is clearly necessary for stability, but need not be sufficient. Once the maximum stable time step is determined, the data for observed line scan images are interpolated in time using cubic splines to obtain intermediate fluorescent profiles in space. This technique fits a smooth cubic curve between two adjacent points in time thus allowing for smaller time stepping in the partial differential equation and increased stability of the numerical scheme.

Step (iv): Conversions to concentrations of CaB_e

It is necessary to convert the fluorescent intensities into concentrations of CaB_e for input into the reaction-diffusion equations. We define

$$\lambda = \frac{[Ca^{2+}(0)]}{[Ca^{2+}(0)] + k_d} \tag{28}$$

$$k_d = \frac{k_e^-}{k_e^+} \tag{29}$$

where λ is the conversion constant, and k_d is the ratio of the dissociation and association constants for CaB_e. Hence, the concentration of CaB_e is

$$[CaB_e(t)] = [B_{e,\mathrm{total}}]\lambda\frac{I(t)}{I(0)} = \frac{[B_{e,\mathrm{total}}][Ca^{2+}(0)]}{[Ca^{2+}(0)] + k_d}\frac{I(t)}{I(0)}, \tag{30}$$

for $I(t)$ the fluorescent intensity, at time t. This equation assumes that fluorescence of B_e, the free form of fluo-3, is negligible [6].

Step (v): The reaction-diffusion equation

The amount of calcium diffusion in heart muscle is governed by a quasi-linear reaction-diffusion equation (Eqs. (1)-(5)). We utilize finite difference approximations which are first order in time and second order in space to discretely approximate the equations. Calculations are solved for all space distances before incrementing time. The mesh size in space (0.15 μm) remains unchanged throughout the calculation.

We model the basic parabolic reaction-diffusion equation

$$u_t + D_B u_{xx} + f(u, x) = 0 \tag{31}$$

by the difference scheme

$$\frac{u_j^{n+1} - u_j^n}{\triangle t} + D_B \frac{u_{j+1}^n - 2u_j^n + u_{j-1}^n}{\triangle x} + f(u_j^n, x_j) = 0. \tag{32}$$

where D_B is the diffusion constant for a mobile species. Since the numerical scheme is explicit, it is subject to stability time step restrictions. In particular, the experimental data is collected at 2 msec time intervals which are too large and hence, unstable in the numerical scheme. The time step must be reduced by a factor of at least 20 and to meet the time step restriction. For this reason, the data is interpolated using a Cubic spline function.

The computational region has net diffusion away from the center. Hence, second-order forward differences are utilized to approximate the second derivative on the left and second-order backward differences are utilized to approximate the second derivative on the right. The numerical problem is subject to instability at the computational boundary due to the rapid changes of the function on the interior of the computational domain. To prevent disturbances of the solution on the interior domain by the instabilities from the boundary, the computational domain is extended by ng cells, termed "ghost cells." Data for the ghost cells is calculated using a Gaussian smoothing function fit to the experimental data (see below). The number of ghost cells which provide a stable and accurate solution is investigated.

Standard inputs which are taken from experimental data include the initial stationary, mobile and exogenous buffer concentrations and the initial free calcium ion concentration. In addition, all buffer rate constants and diffusion coefficients are recorded. The catalyst of the reaction-diffusion computation is the output of the cubic spline code (the parameters found as a result of the cubic spline interpolation) which calculate the value of the exogenous calcium-bound fluorescent buffer CaB_e.

The mass of calcium is calculated in three dimensions by

$$\mathrm{Ca}_{\mathrm{mass}} = \frac{4}{3}\pi[(r_i^+)^3 - (r_i^-)^3]\frac{[Ca^{2+}(x_i)] + [Ca^{2+}(x_{-i})]}{2} \tag{33}$$

where $r_i^+ = i\triangle x + (\triangle x/2)$, $r_i^- = i\triangle x - (\triangle x/2)$, $\mathrm{Ca}(x_i)$ and $\mathrm{Ca}(x_{-i})$ are the concentrations of calcium computed at nodes x_i and x_{i-}, respectively and $\mathrm{Ca}_{\mathrm{mass}}$ defines the mass in a spherical shell of width $\triangle x$ about x_i.

3.1 Testing Algorithms

Utilizing the five-step algorithm, we address the efficacy and efficiency of this algorithm. The first test is to analyze results obtained via direct deconvolution of raw experimental data and determine the need, if any, for idealization of raw experimental data prior to deconvolution. As part of this test, we determine the effects of subtracting baseline prior to deconvolution of smooth data. To create a control, $F = Gg$, the smooth image of a known, idealized object, let g be a Gaussian idealized object and let ng be the number of ghost cells to be added. Add ng ghost cells on each boundary in the x direction for each time t. Convolve with G to get the control, F. Perform one of the following tests on F:

T1 Deconvolve smooth F without subtracting baseline by solving $\tilde{g} = G^{-1}F$. Remove ghost cells and compare $\tilde{g}$ with g to get the root-mean-square error (RMS) for each time step.

T2 Before deconvolution, subtract the baseline off the smooth image to create F_{-b}, and solve $\tilde{g} = G^{-1}F_{-b}$. Add the baseline back after calculation, remove ghost cells and compare $\tilde{g}$ with g to get the RMS error for each time step.

Next, we determine the effects of subtracting baseline prior to deconvolution of raw (experimental) data. Create the control, F. Randomly generate noise at signal to noise ratios of 2 - 1 to 100 - 1 to create F^{+n}. Perform one of the following tests on F^{+n}:

T3 Deconvolve the raw data F^{+n}.

- **a** Directly deconvolve F^{+n} to get $\tilde{g}$. Remove ghost cells and compare $\tilde{g}$ with g to get the RMS error for each time step.
- **b** Before deconvolution, subtract the baseline off the raw image to create F^{+n}_{-b}, run through the deconvolution program, and then add the baseline back after calculation. Remove ghost cells and compare $\tilde{g}$ with g to get the RMS error for each time step.

T4 Idealize the raw data F^{+n} prior to deconvolution using SigmaPlot© software and obtain parameters for the amplitude, A, standard deviation, σ, the mean, m, and the offset value d_{off}, which fit F^{+n} to the Gaussian

$$\mathcal{F}(x) = \frac{\mathrm{e}^{(x-m)^2/\sigma^2}}{\sqrt{2\pi}\sigma} - d_{\text{off}}. \tag{34}$$

Discretize $\mathcal{F}(x)$ over the spatial grid.

- **a** Directly deconvolve $\mathcal{F}$ to get $\tilde{g}$. Remove ghost cells and compare $\tilde{g}$ with g to get the RMS error for each time step.
- **b** Before deconvolution, subtract the baseline off the image to create $\mathcal{F}_{-b}$, run through the deconvolution program, and then add the baseline back after calculation. Remove ghost cells and compare $\tilde{g}$ with g to get the RMS error for each time step.

As a consequence of this test, we are able to determine the sensitivity of the solution to the amount of signal noise added to idealized and non-idealized spark data. Noise is added to the spark as follows:

$$\text{noise} = \frac{\text{signal}}{\text{s}} * (\text{random} \pm 0.5) \tag{35}$$

$$\text{value} = \text{signal} + \text{noise}, \tag{36}$$

where $s,\ 1 \leq s \leq 500$, is a multiplier which determines the magnitude of the noise. The average value error E_{avg} (see Eq. (38)) of solutions with and without idealization as compared to the exact solution is computed.

The second test is to determine the effects of filtering the image prior to deconvolution. The deconvolved object is the amount of the calcium-bound fluorescent ion, CaB_e, which are used as the catalyst in the reaction diffusion equations which calculate total Ca^{2+}. During the deconvolution process, numerical errors are introduced at the boundary of the computational domain which propagate into the interior and degrade the solutions. Hence, numerical errors are to be avoided.

To simulate real image properties, create the control, F, and add signal noise to create F^{+n}. Perform one of the following tests on F^{+n}:

T5 Idealize noisy data using SigmaPlot© software and obtain parameters A, σ, m, and d_{off}. Create an idealized image of the noisy data, $\mathcal{F}$. Directly deconvolve $\mathcal{F}$ to get $\tilde{g}$. Remove ghost cells and compare $\tilde{g}$ with g to get the RMS error for each time step.

T6 Filter noise data:
Filter the data using a low-pass $N \times 1$ grid to average the data over N points to create $F^{+(n,f)}$. Directly deconvolve $F^{+(n,f)}$ to get $\tilde{g}$. Remove ghost cells and compare $\tilde{g}$ with g to get the RMS error for each time step.

We utilize three different error approximations to evaluate the results. These approximations are defined below:

$$S_{\text{error}} = \frac{\sum\sum |x_{ij}^c - x_{ij}|}{\sum\sum x_{ij}} \tag{37}$$

$$E_{\text{avg}} = \frac{\sum\sum |x_{ij}^c - x_{ij}|}{(nx+1)(nt+1)} \tag{38}$$

$$RMS = \frac{\sqrt{\sum\sum |x_{ij}^c - x_{ij}|^2}}{(nx+1)(nt+1)} \tag{39}$$

where x_{ij}^c is the computed value, x_{ij} are the true values, and S_{error}, E_{avg} and RMS are the SumPercentError, the AverageValueError and the RootMeanSquare error, respectively.

The third test is to determine the linearity effects of the mobile exogenous Ca^{2+}-bound buffer CaB_e on the total amount of calcium mass. The value of the dissociation constant k_e^- was varied from high to low ranges respectively, in the interval [.24, 1.5] msec^{-1}, derived from *in vitro* and *in situ* calibrations of the exogenous buffer B_e, fluo-3. The total Ca^{2+} was

computed for different amplitudes for each value of k_e^- and the linearity of the solution was examined. Linearity effects are determined for masses of total calcium, and the calcium-bound buffers.

Lastly, as a verification of the accuracy of the code, a complete evaluation is performed for an idealized spark (test data) and for the raw spark data (experimental, idealized). The total mass of each ion is determined and plotted.

4 Numerical Results

In this section, we present results describing the effectiveness of the numerical method in three dimensions. Since the solutions are symmetric with respect to x, y and z the solution can be calculated in three dimensions.

The following constants were set in the program:

$$\sigma_{xy} = 0.173, \qquad \sigma_z = 0.515 \tag{40}$$

$$B_{s,\text{total}} = 123.0, \qquad B_{m,\text{total}} = 4700.0, \qquad B_{e,\text{total}} = 820.0, \qquad Ca^0 = 0.1, \tag{41}$$

$$k_s^+ = 0.10 \qquad k_m^+ = 0.0015 \qquad k_e^+ = 0.600, \tag{42}$$

$$k_s^- = 0.096, \qquad k_m^- = 0.0003, \qquad k_e^- = .24, 1.5, \tag{43}$$

$$D_{Ca} = 0.250, \qquad D_{B_m} = 0.113, \qquad D_{B_e} = 0.095, \tag{44}$$

$$nx = 22, \qquad nt = 22, \qquad ng = 8, \qquad dx = 0.15. \tag{45}$$

Here, σ_x is the standard deviation in x for the PSF in μm, σ_z is the standard deviation in z for the PSF in μm, $B_{i,\text{total}}$ is the total buffer concentration for $i = s, m, e$ in micromolar (μM), Ca^0 is the initial free calcium ion concentration in μM, k_s^+ is the stationary association constant, k_m^+ is the mobile association constant, and k_e^+ is the mobile exogenous association constant in msec$^{-1}\mu$M^{-1}, k_s^- is the stationary dissociation constant, k_m^- is the mobile dissociation constant, and k_e^- is the exogenous dissociation constant in msec^{-1}, D_{Ca} is calcium diffusion coefficient, D_{B_m} is the mobile buffer diffusion constant and D_{B_e} is the mobile exogenous buffer diffusion constant in μm^2/msec, nx is the number of x points, nt is the number of t points, and ng is the number of ghost cells.

We assume the diffusion constants $D_{CaB_m} = D_{B_m}$ and $D_{CaB_e} = D_{B_e}$ [3, 6, 9, 11, 12]. The association and dissociation constants of Ca^{2+} buffering species are not known in the environment of the cytosol. These constants can be estimated, however, from the equilibrium binding constants (k_d) that have been determined in the cytosol for B_s [2] and B_e [6] and from known Ca^{2+} chelating properties of other exogenous buffers, B_m. In this calculation, B_e, is given a diffusion-limited association constant (k_e^+) because of its previously determined properties [6], while B_s is assumed to have a somewhat slower constant (k_s^+) due to the immobile nature of endogenous buffers. On the other hand, B_m (in this case the chelator EGTA) is known to have much slower Ca^{2+} binding kinetics [10]. These association constants along with k_d allow for an estimation of the dissociation constant for each Ca^{2+} buffering species (equation (29)).

Error	Idealized	Filter 3×1	Filter 5×1	Filter 7×1
SumPercent	0.22773	0.80812	0.53981	0.48819
AverageValue	8.71480	30.92508	20.65740	18.68192
RootMeanSquare	0.96802	2.00653	1.45333	1.29004

Table 1: Errors obtained when idealization or filtering is performed prior to deconvolution.

In the first test, we calculated and analyzed the results obtained via direct deconvolution of smooth and experimental data when idealization of the data is and is not performed prior to deconvolution. First, we calculated the deconvolved object of a smooth image as is and second, we calculated the deconvolved object after subtracting the baseline from smooth data to determine the preferred method. Results show that when we do not subtract baseline from the smooth deconvolved image, we obtain a RMS error of 1.99E-13. Computation of the RMS error on solutions obtained after baseline subtraction yields an error of 0.26989.

Next, we add noise to the smooth image to create raw data, similar to that obtained experimentally. We calculated and analyzed the results obtained via direct deconvolution of raw (experimental) data and results obtained when idealization of the data to smooth data via a Gaussian, is and is not performed prior to deconvolution. First, we calculated the deconvolved object of the raw image. Results show that when we do not subtract baseline from the raw non-smooth image, we obtain a RMS error of 10.48242. Computation of the RMS error on solutions obtained after baseline subtraction yield error of 10.49261. Prior to the following computations, we idealized the raw (experimental) data to smooth data and calculated the deconvolved object of the smooth image. Results show that when we do not subtract baseline from the idealized image, we obtain a RMS error of 0.42158. Computation of the RMS error on solutions obtained after baseline subtraction from the idealized image yields an error of 0.30106. Therefore, the smallest value of RMS error is obtained when baseline subtraction occurs prior to the deconvolution of an idealized image.

We tested the solutions sensitivity to the signal to noise ratio and obtained very small values of E_{avg} when idealization is performed prior to deconvolution. Figures 3a and 3b depict the decrease in E_{avg} for different signal noise values for non-idealized and idealized Ca^{2+} sparks, respectively.

We tested the accuracy of the solution when idealization or filtering is performed prior to deconvolution. Table 1 depicts the error for each test according to the three different error estimates. According to all three errors, it is clear that the smallest error is obtained when the data is idealized, not filtered.

Next, we examine the sensitivity of the accumulation of Ca^{2+} mass with regard to the dissociation constant k_e^- for the exogenous mobile calcium-bound buffer CaB_e. Figure 4 is a plot of the mass of total calcium (Ca^{2+}_{total}) with respect to varying amplitude for the high and low affinity buffers assuming a dissociation constant of 0.4 μM and 2.5 μM which are in vitro and in situ dissociation constants, respectively [6]. Tables 2 and 3 display the increase in mass for Ca^{2+}-bound exogenous species, CaB_e.

In this calculation, it was also observed that increasing the number of ghost cells from four to eight at each boundary significantly decreased numerical oscillations at the boundary of the

Ca^{2+} spark amplitude	moles $\times 10^{21}$				
	Ca^{2+}	CaB_e	CaB_m	CaB_s	Sum
6.7	0.02719	9.89141	2.09403	1.13142	13.14405
13.4	0.05439	19.78355	4.18928	2.25796	26.28517
27	0.10783	38.80133	7.61759	4.04664	50.57338
54	0.21795	79.26338	16.75918	8.91342	105.15394
107	0.43541	158.31274	32.34306	17.31776	208.40897

Table 2: Sum represents the total amount of calcium mass for varied spark amplitudes; t = 24.3; ($k_e^- = 1.5$)

Ca^{2+} spark amplitude	moles $\times 10^{21}$				
	Ca^{2+}	CaB_e	CaB_m	CaB_s	Sum
6.7	0.026679	51.73239	2.03690	1.08979	54.88576
13.4	0.053364	103.46890	4.07507	2.17496	109.77229
27	0.106894	207.23730	8.15098	4.33157	219.82674
54	0.213845	414.49059	16.30346	8.58677	439.59466
107	0.427453	828.28505	31.43653	16.67700	876.82604

Table 3: Sum represents the total amount of calcium mass for varied spark amplitudes; t = 24.3; ($k_e^- = 0.24$)

true spark domain. We next determined the total amounts of Ca^{2+}, CaB_e, CaB_s, and CaB_m using an *idealized spark* created for computations only to validate results when the solution is known. Figures for Ca^{2+}, CaB_s and CaB_m are omitted due to space limitation.

Figures (5a) and (5b) provide comparative results describing the mass of CaB_e, the calcium-bound exogenous mobile buffer obtained using high and low affinity buffers, respectively.

Of most importance are the computations which utilize an averaged raw (experimental) spark. To demonstrate the effectiveness of this technique, we determined the calcium concentration, $[Ca^{2+}]$, the masses of Ca^{2+}, CaB_e, CaB_s, and CaB_m using an averaged idealized spark created from several calcium sparks. Figure (6) is a one dimensional plot of an average Ca^{2+} spark in time and space prior to idealizational. The figure represents fluorescent intensities of the calcium bound buffer CaB_e which is the catalyst for the reaction-diffusion equations (1) – (6). Figure (7) is a one dimensional plot of the deconvolved average Ca^{2+} spark after idealization to a Gaussian function is performed. Figure 8 is a one dimensional plot of the free calcium ion concentration calculated after conversion of the Ca^{2+} spark to $[CaB_e]$ (Eq. (30)) and solution of the reaction-diffusion equations (1) – (5). In figure (9), the mass of free Ca^{2+} is observed and presented for each time in terms of the moles of Ca^{2+} versus the radial distance from the center of the spark as a function of time. Figures (10) – (12) are one-dimensional plots of the mass of calcium-bound mobile and stationary buffers, CaB_m, CaB_e, and CaB_s. Note that the mass of all Ca^{2+}-bound species moves a significant distance away from the origin as time progresses.

5 Discussion

Using a Five-step algorithm, we have shown that the baseline should not be subtracted prior to deconvolution of smooth data. However, when we add noise to the convolved image and idealize the non-smooth data, subtracting the baseline prior to deconvolution gives more accurate results after deconvolution. When we add noise to the convolved image and do not idealize the noise image, both subtraction and no subtraction baseline give poor results. Hence, once noise is introduced, it is necessary to idealize the data prior to further analysis. Therefore, in practical situations, it is necessary to idealize experimental data before the data is deconvoluted. In comparing the average value error between idealization and no idealization for each ratio, it is clear that idealization is absolutely necessary in order to reduce errors to acceptable levels.

We have determined that smallest error arises from data idealization of the image prior to deconvolution as opposed to data filtering. Even with filtering, one can not reduce error to acceptable levels without losing needed spatial information.

While the degree of Ca^{2+} binding increases with higher affinity buffers, saturation of a significant fraction of total buffers does not occur under the conditions encountered over the time and space of a Ca^{2+} spark in the face of high exogenous buffer concentrations (see Figure (4)). Theoretically, as the degree of saturation increases and a significant fraction of the buffer becomes bound to the Ca^{2+}, total calcium mass increases nonlinearly. Although saturation is known to take place for highly-bound buffers, it is not physically observable in the figure. These nonlinear effects significantly increase the difficulty of calculations for the reaction-diffusion equation. Irregardless of the buffer, changes in fluorescence are small and are only reflected in the mass of CaB_e and the total sum of calcium. Hence, we can choose buffers of different affinities since the qualitative information is valid. We can conclude that for our final tests, we can use high affinity Ca^{2+} buffers without significant errors in calculating the mass of Ca^{2+} involved in a Ca^{2+} spark.

The calculation of the total mass of calcium provides a measure of the total mass of calcium involved in the release from the SR (sarcoplasmic reticulum). This information simulates how excitation-contraction coupling regulates individual release events which make up the cytosolic calcium transient. Calcium transients control the contraction of heart muscle thus providing information regarding pathological and diseased states.

Acknowledgments

This research was supported in part by the National Science Foundation grant DMS 98-03605 (D.A. Lott), the Foundation at the New Jersey Institute of Technology (D.A. Lott), by National Institutes of Health grants HL 43712 (J.R. Berlin) and HL 69020 (J.R. Berlin). M. Li was supported in part by the McNair Scholarship Program. The authors thank the Center for Applied Mathematics and Statistics and the Department of Mathematical Sciences at NJIT and the Department of Pharmacology and Physiology at UMDNJ for research facilities.

References

[1] D. A. Agard, Y. Hiraoka, P. Shaw, J. W. Sedat, 1989. Fluorescence Microscopy in Three Dimensions. Methods in Cell Biology **30**, 353 – 377.

[2] J. R. Berlin, J. W. M. Bassani, D. M. Bers, 1994. Intrinsic cytosolic calcium buffering properties of single rat cardiac myocytes. *Biophys. J.* **67**, 1775 – 1787.

[3] L. A. Blatter, J. Hüser, E. Ríos, 1997. Sarcoplasmic reticulum Ca^{2+} release flux underlying Ca^{2+} sparks in cardiac muscle. *Proc. Natl. Acad. Sci.* **94**, 4176 – 4181.

[4] M. L. Collier, A. P. Thomas and J. R. Berlin, 1999. Relationship between L-type Ca^{2+} current and unitary sarcoplasmic reticulum Ca^{2+} release events in rat ventricular myocytes. *J. Physiol.* **516**, 117 – 128.

[5] A. González, W. G. Kirsch, N. Shirokova, G. Pizarro, M.D. Stern, E. Ríos, 2000. The spark and its ember. *J. Gen. Physiol.* **115**, 139 – 157.

[6] A. B. Harkins, N. Kurebayashi, S.M. Baylor, 1993. Resting myoplasmic free calcium in frog skeletal muscle fibers estimated with fluo-3. *Biophys. J.* **65**, 865 – 881.

[7] Y. Hiraoka, J. W. Sedat, D. A. Agard, 1990. Determination of three-dimensional imaging properties of a light microscope system. *Biophys. J.* **57**, 325 – 333.

[8] M. Kulkarni, T. Belytschko, A. Bayliss, 1995. Stability and error analysis for time integrators applied to strain softening materials. *Comp. Meth. Appl. Mech. Eng.* **124**, 335 – 63.

[9] E. Ríos, M. Stern, A. González, G. Pizarro, N. Shirokova, 1999. Calcium release flux underlying Ca^{2+} sparks of frog skeletal muscle. *J. Gen. Physiol.* **114**, 31 – 48.

[10] P. D. Smith, G. W. Liesegang, R. L. Berger, G. Czerlinski, R. J. Podolsky, 1984. A stopped-flow investigation of calcium ion binding by ethylene glycol bis(β-aminoethylether)-*N,N*'-tetraacetic acid. *Anal. Biochem.* **143**, 188 – 195.

[11] G. D. Smith, J. Wagner, J. Keizer, 1994. Validity of the rapid buffering approximation near a point source of calcium ions. *Biophys. J.* **70**, 2527 – 2539.

[12] J. Wagner, J. Keizer, 1994. Effects of rapid buffers on Ca^{2+} diffusion and Ca^{2+} oscillations. *Biophys. J.* **67**, 447 – 456.

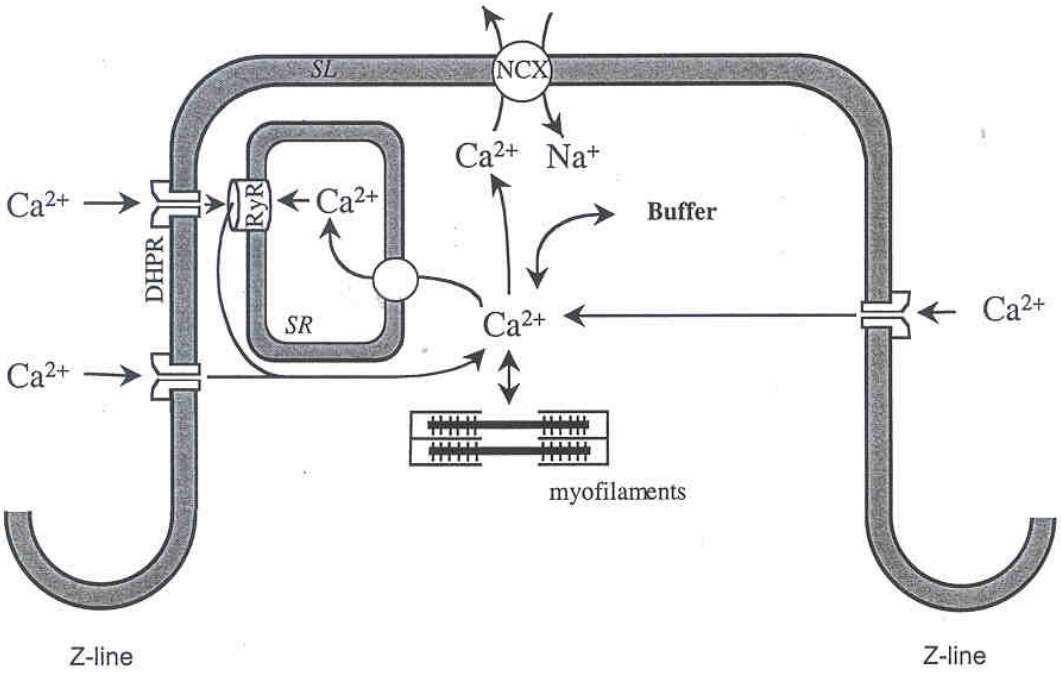

Figure 1:
Ca $^{2+}$ fluxes contributing to excitation-contraction coupling in cardiac myocytes.

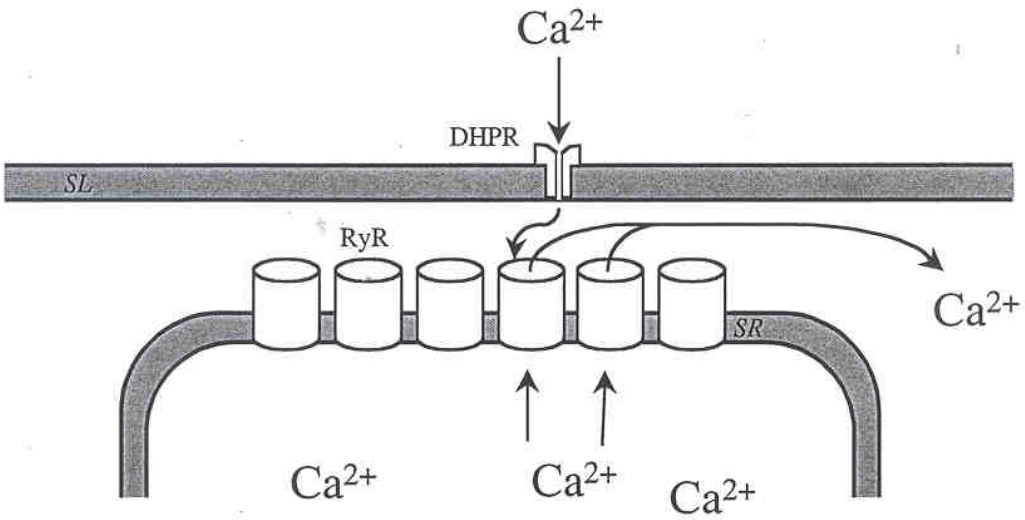

Figure 2: The subcellular junction involved in excitation-contraction coupling.

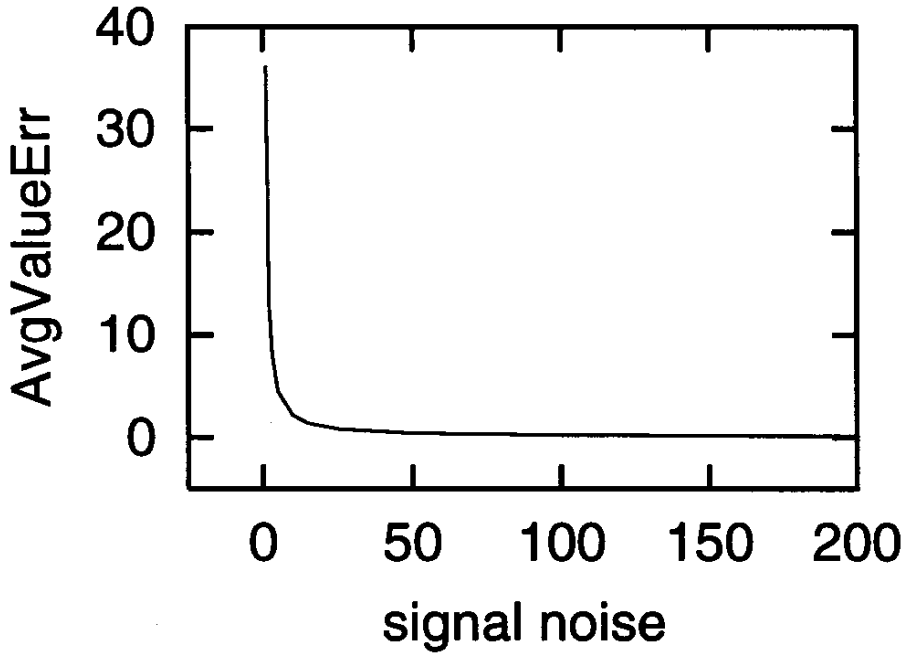

Figure 3a: Average value error versus signal noise for non-idealized spark data.

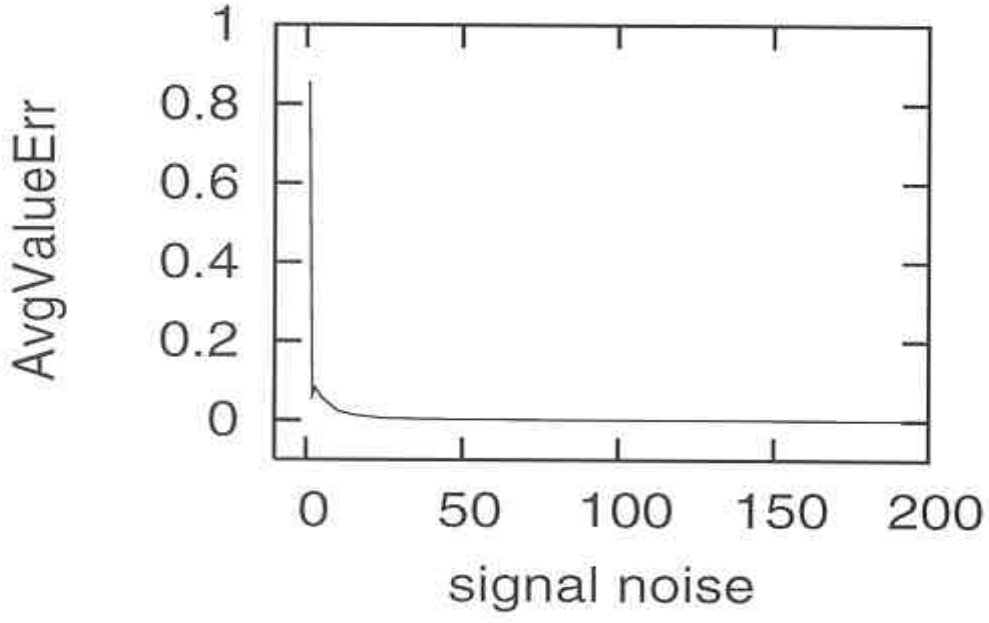

Figure 3b: Average value error versus signal noise for idealized spark data.

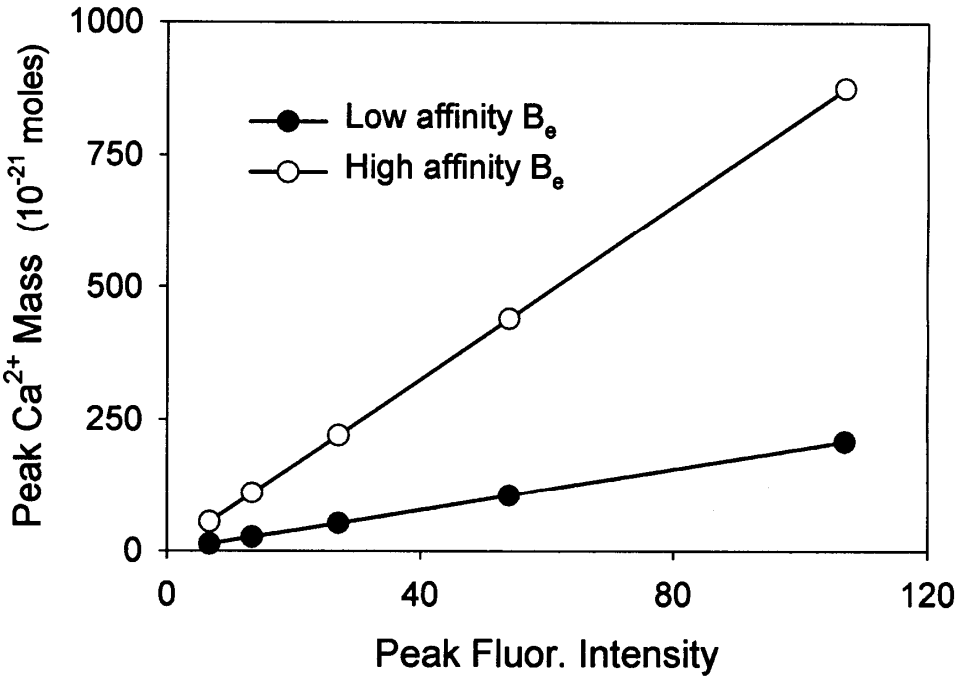

Figure 4:
Total calcium mass with respect to amplitude of the fluorescence for high and low affinity buffers.

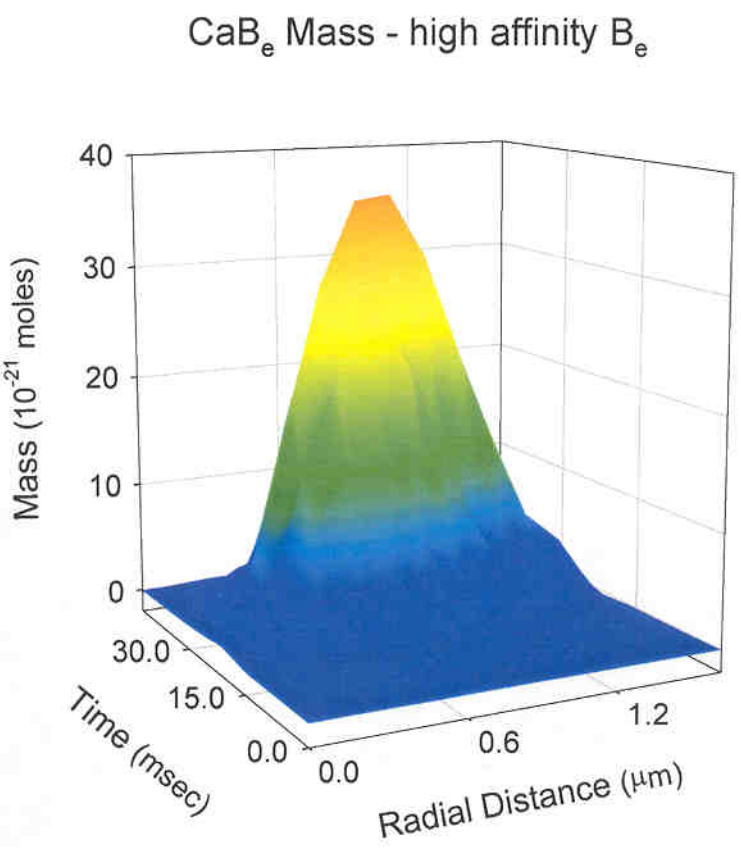

Figure 5a:
The mass of CaB_e as a function of time and space with a high-affinity buffer.
Distance is provided in reference to the center of the spark.

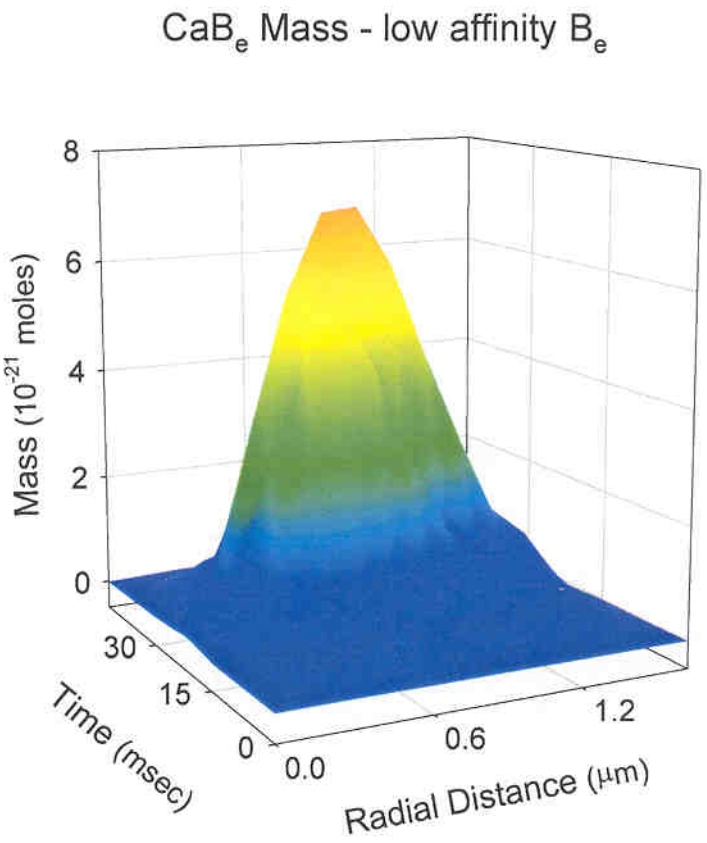

Figure 5b:
The mass of CaB_e as a function of time and space with a low-affinity buffer. Distance is provided in reference to the center of the spark.

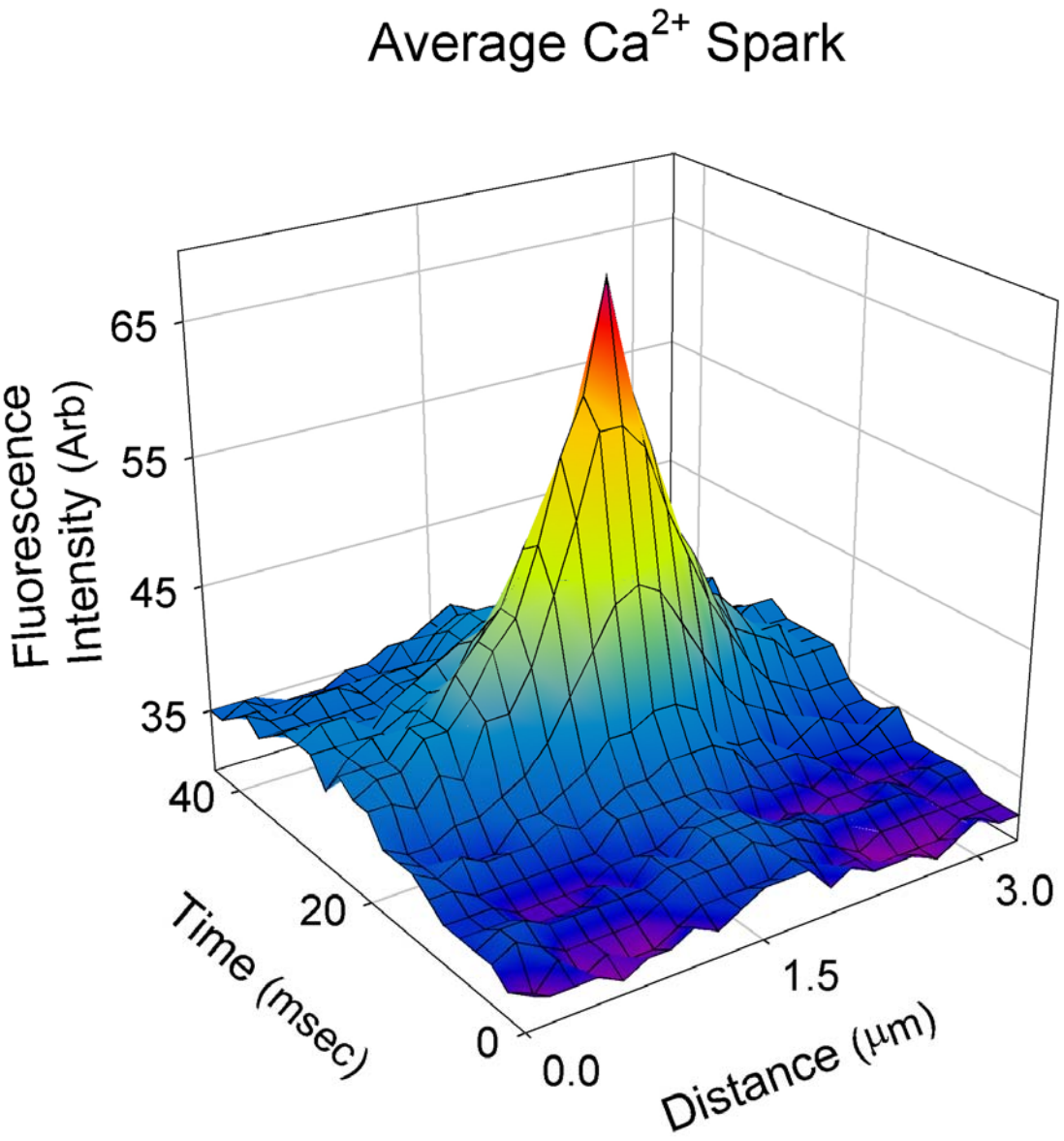

Figure 6:
An averaged calcium spark prior to idealization. Results shown are from images determined via confocal microscopy. The peak of several line scans are aligned and the data from each scan averaged.

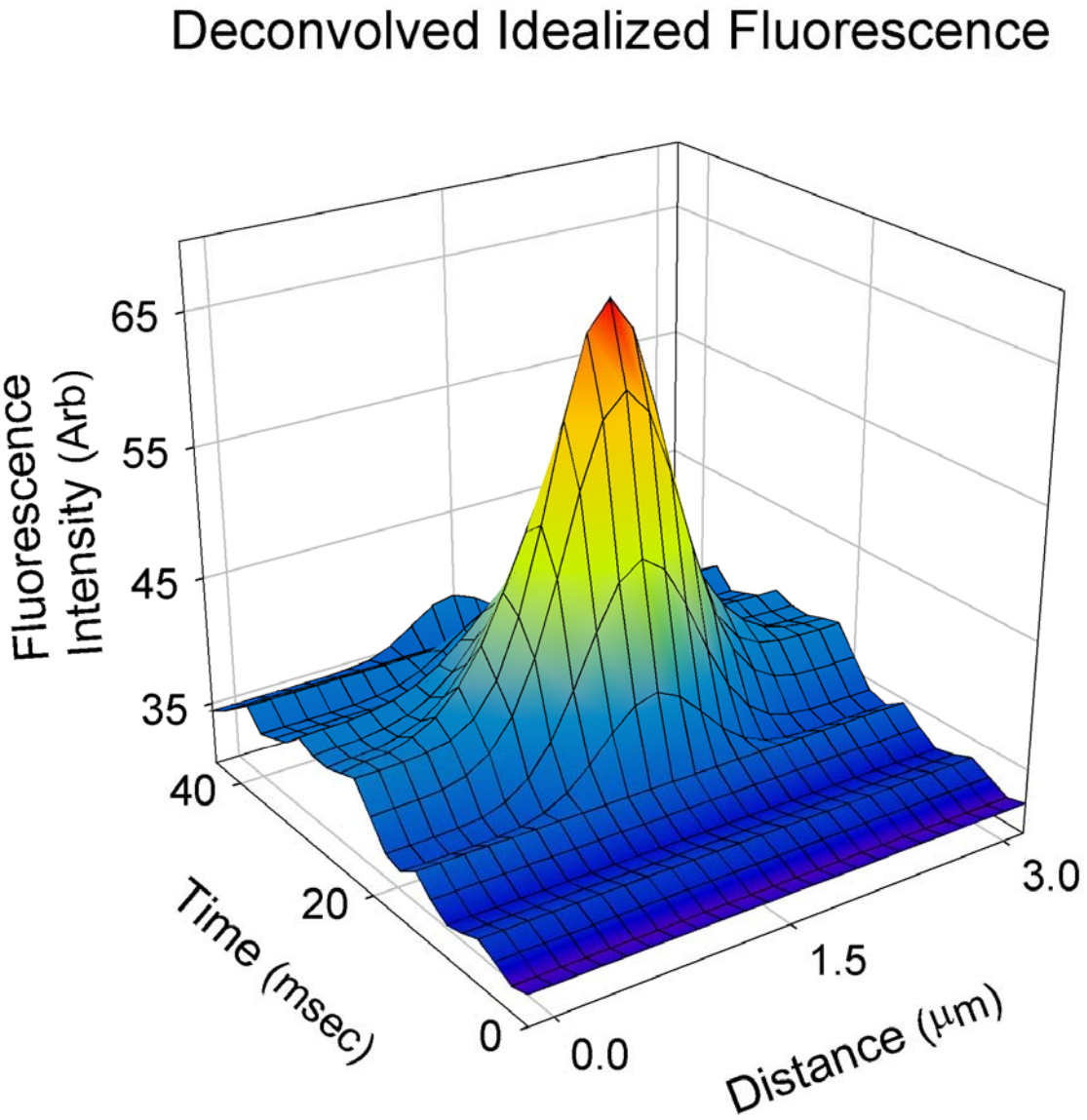

Figure7:
A deconvolved, averaged calcium spark after idealization to a Gaussian function at each experimental time point.

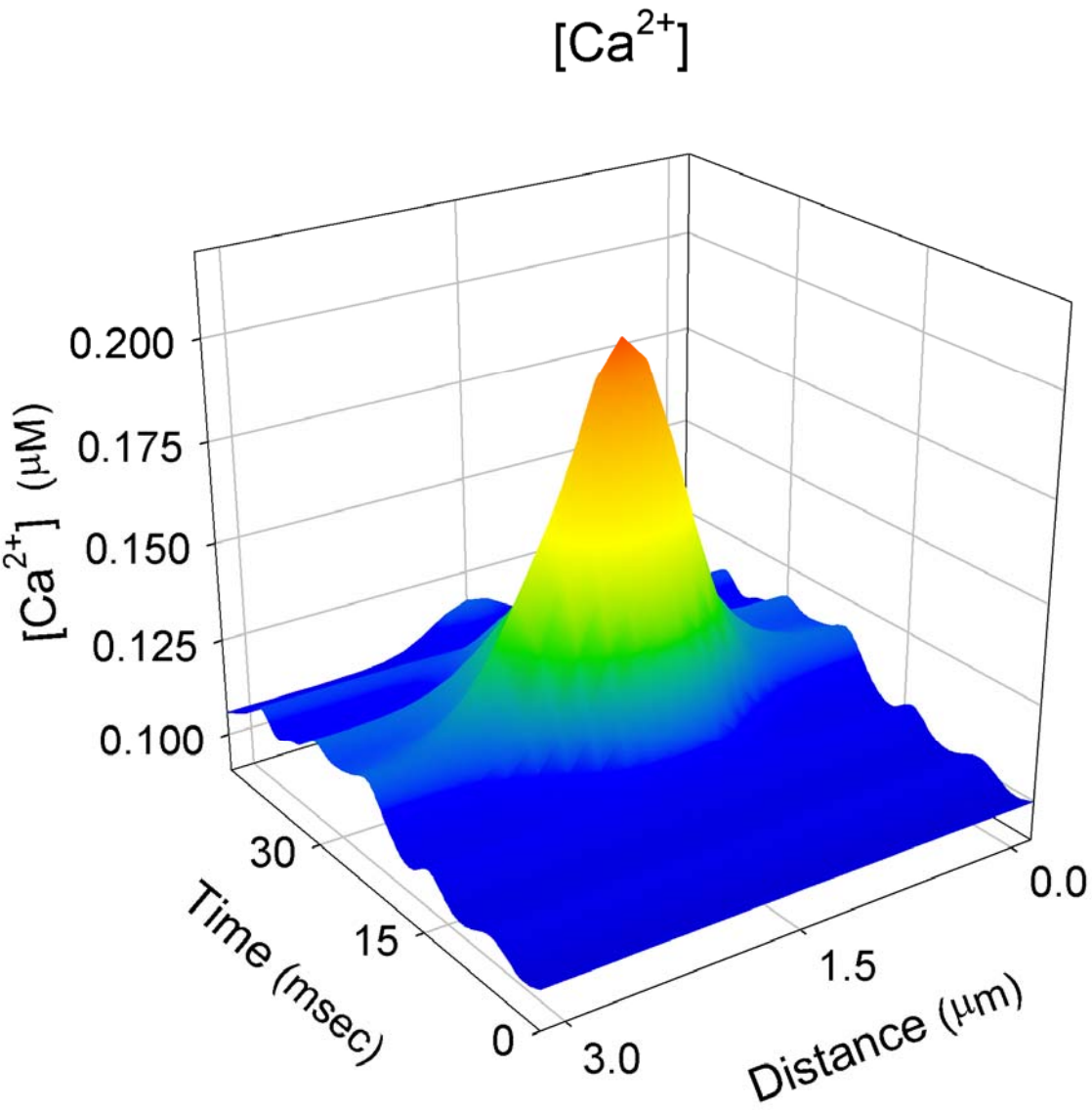

Figure 8: The initial concentration of calcium.

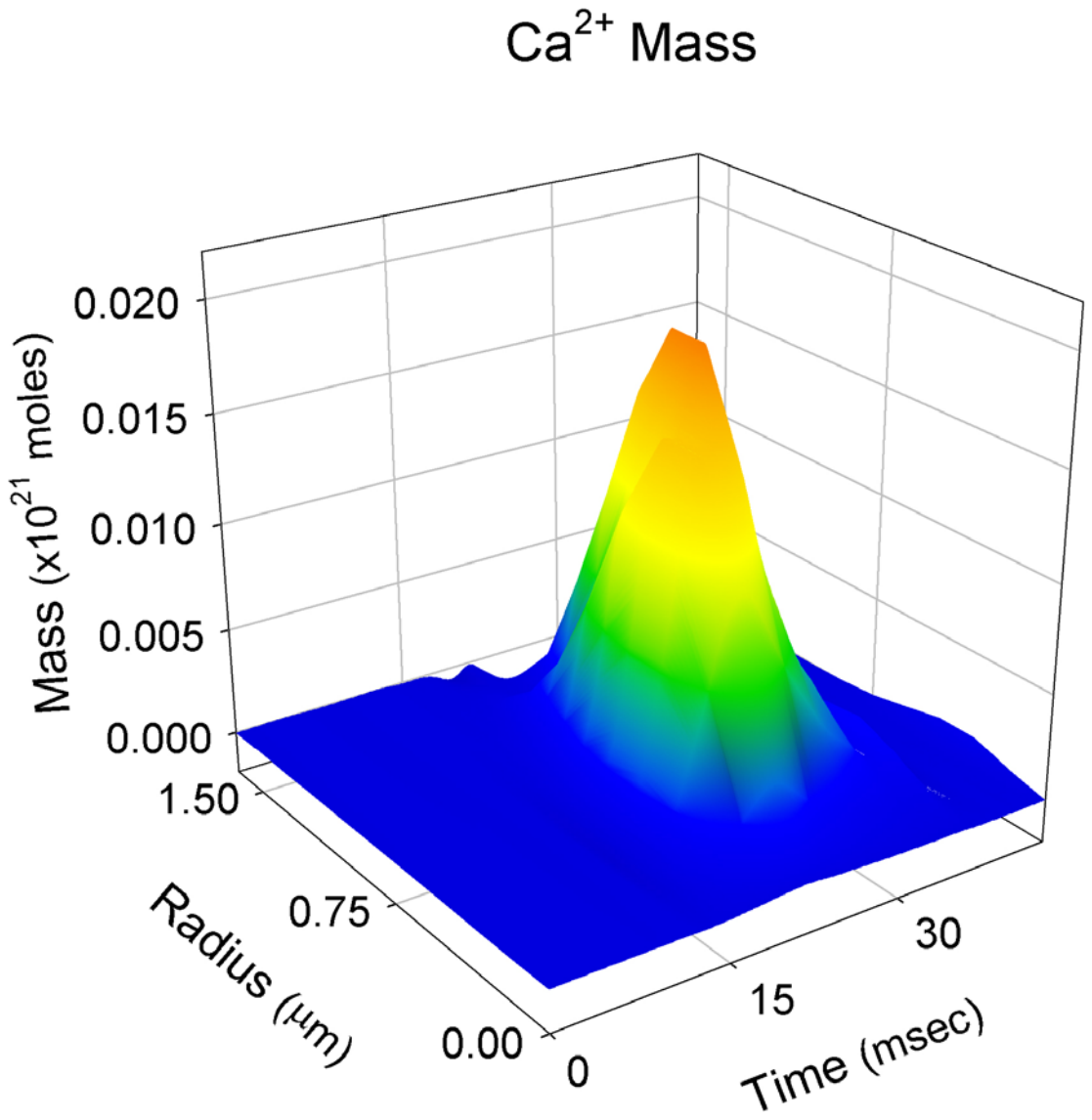

Figure 9:
The mass of Ca^{2+} as a function of time and space.
Distance is provided in reference to the center of the spark.

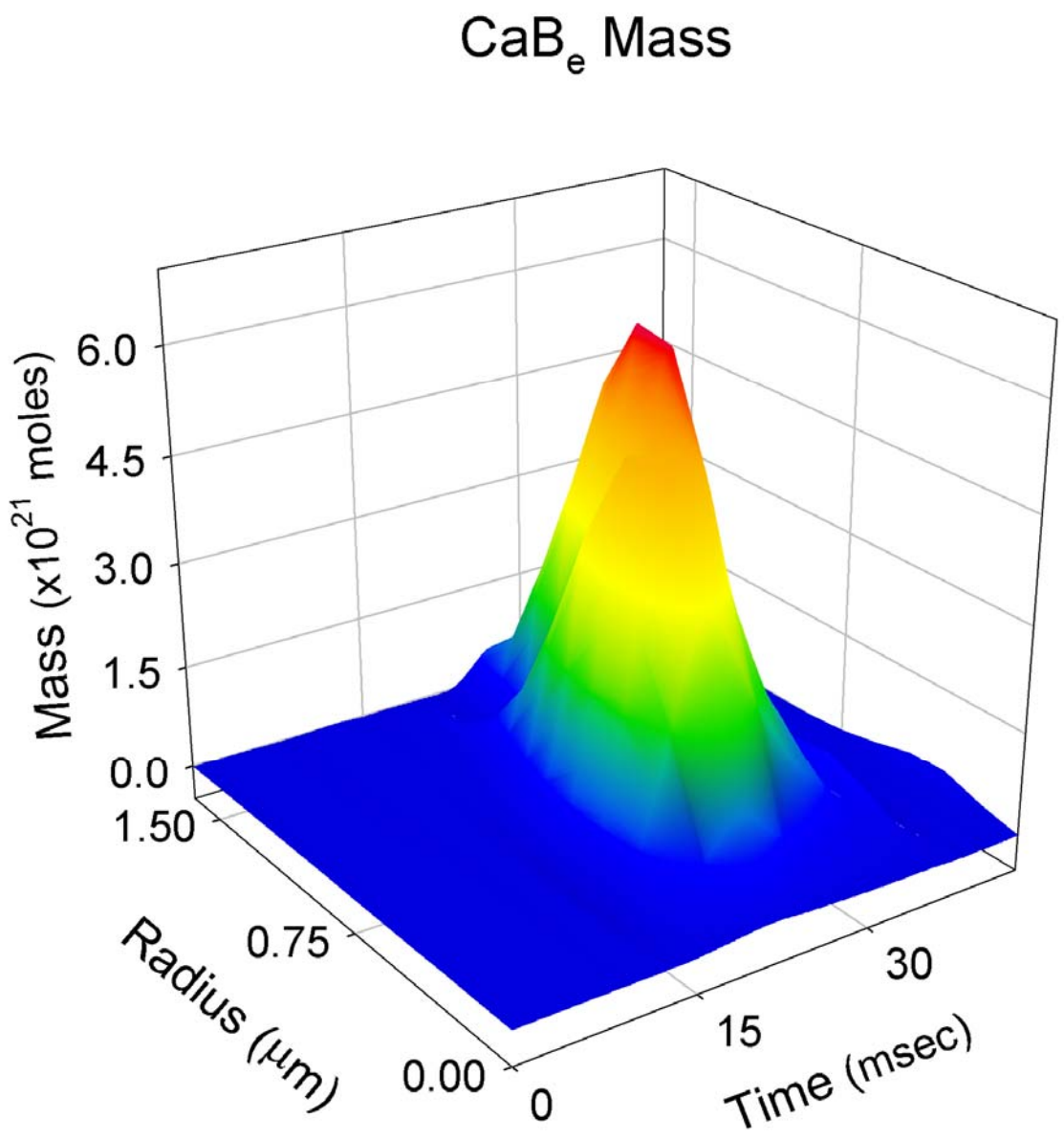

Figure 10:
The mass of CaB_e as a function of time and space.
Distance is provided in reference to the center of the spark.

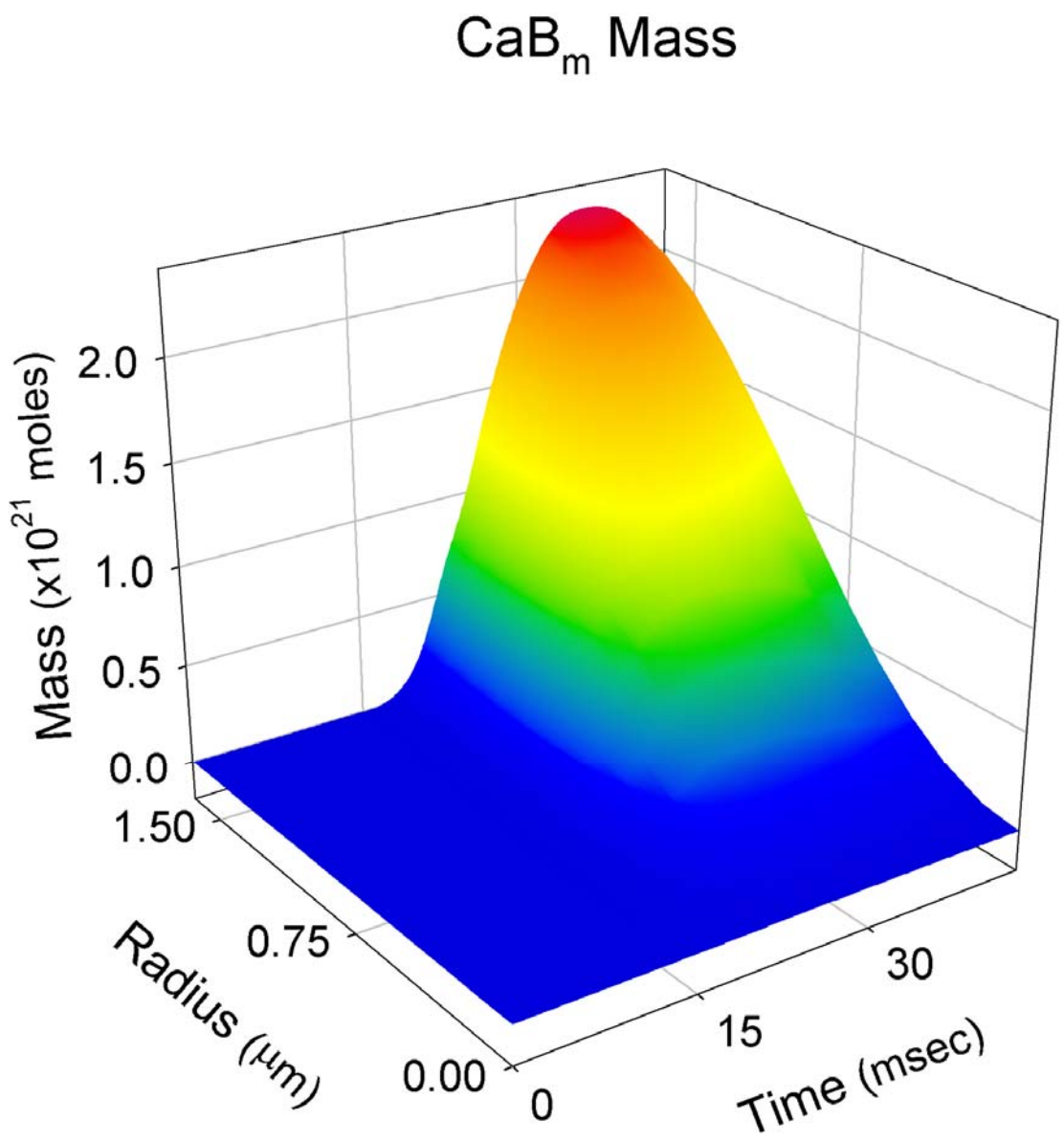

Figure 11:
The mass of CaB_m as a function of time and space.
Distance is provided in reference to the center of the spark.

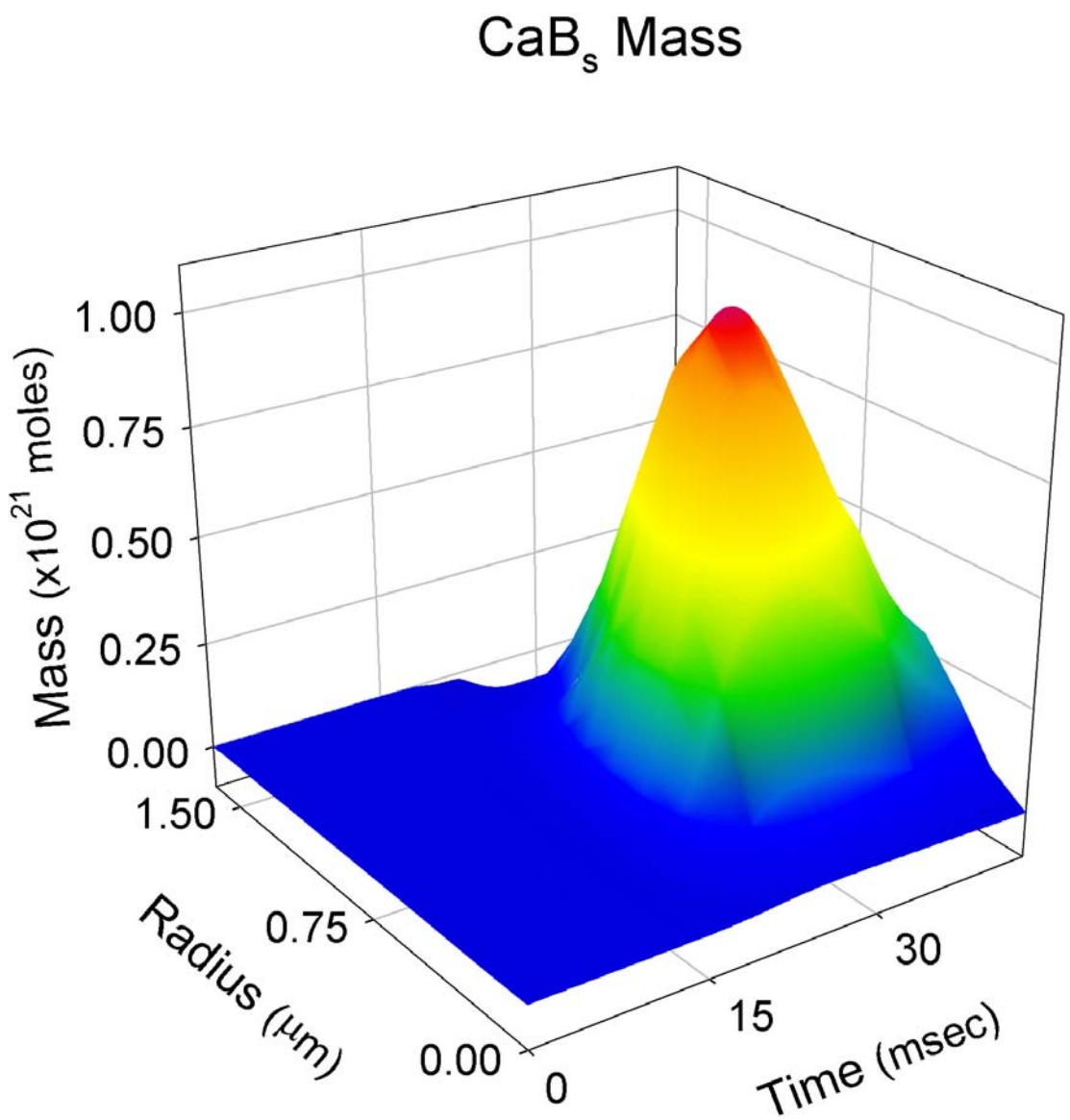

Figure 12:
The mass of CaB_s as a function of time and space.
Distance is provided in reference to the center of the spark.